Relationship between Absorbance Spectra and Particle Size Distributions for Quantum-Sized Nanocrystals

Noshir S. Pesika,[†] Kathleen J. Stebe,[†] and Peter C. Searson*[,‡]

Department of Chemical & Biomolecular Engineering, and Department of Materials Science & Engineering, Johns Hopkins University, Baltimore, Maryland 21218

Received: March 10, 2003; In Final Form: June 19, 2003

The shape of the absorbance edge for a suspension of semiconductor quantum particles is influenced both by the electronic transition and the distribution of band gaps in the system. Using a suitable model to relate the absorption energy to the particle radius, we demonstrate this relationship by inferring the particle size distribution from the absorbance spectrum of a suspension of ZnO quantum particles, and comparing it to the distribution obtained from transmission electron microscope images. This analysis is broadly applicable to quantum particle suspensions of many of the II−VI or III−V compound semiconductors.

Introduction

When the physical dimensions of a solid particle are less than a characteristic length scale of interest, such as the exciton diameter or the electron mean free path, the properties can be significantly different from those of the bulk material. Since the characteristic lengths are usually in the nanometer size regime, particles smaller than about 10 nm often exhibit size-dependent optical, electrical, and magnetic properties. For example, when the size of a semiconductor particle becomes smaller than the exciton diameter, quantum confinement leads to a size-dependent blue shift in the absorbance spectrum. This blue shift is frequently used to demonstrate quantum size effects in suspensions of semiconductor nanoparticles.[1−5] The band gap of the material can be related to the particle size using a suitable model for the confinement,[6−10] and hence the average particle size in a suspension of semiconductor nanoparticles can be obtained from the absorption onset. This feature has been used to determine the evolution of the average particle size due to growth and coarsening.[11−18]

For a bulk semiconductor, the shape of the absorption spectrum in the vicinity of the absorption edge is determined by the nature of the electronic transition from the top of the valence band to the bottom of the conduction band.[19] For an ensemble of semiconductor nanoparticles in the quantum size regime, the shape of the absorption edge is also dependent on the particle size distribution and hence the distribution of band gaps. However, if the particle size distribution is sufficiently large, then the shape of the absorbance spectrum near the onset is dominated by the particle size distribution. In this paper we confirm this relationship by comparing the particle size distribution of a suspension of ZnO quantum particles obtained from the deconvolution of the absorption spectra to the distribution obtained directly from transmission electron microscope images.

Experimental Section

Materials. ZnO nanoparticles were synthesized from $Zn(CH_3CO_2)_2 \cdot 2H_2O$ (Aldrich, reagent grade) and NaOH (Aldrich, conductivity grade). Octanethiol (Aldrich, 98.5% purity) was used to quench the growth of the nanoparticles, and 2-propanol (Aldrich, ACS grade) was used as the solvent for particle growth. (0001)ZnO single crystals (Grade I, of dimensions 10 mm × 10 mm × 0.5 mm) were purchased from Eagle Pitcher. All glassware was soaked in 18 M sulfuric acid overnight and rinsed with distilled and deionized water prior to use. Water was distilled and deionized using a Millipore Milli-Q 50 Purification System (Bedford, MA), which had a resistivity ≥ 18.0 MΩ cm. In all experiments, the chemicals were used as received.

Particle Synthesis. ZnO nanoparticles were synthesized by precipitation from alcohol.[11−20] The overall reaction used here can be written as follows:

$$Zn(CH_3CO_2)_2(l) + 2NaOH(l) \rightarrow ZnO(s) + H_2O(l) + 2NaCH_3CO_2(l)$$

For a typical synthesis, 1.0 mmol of zinc acetate dihydrate was dissolved in 80.0 mL of 2-propanol under constant stirring at 50 °C. Separately, a 0.02 M solution of NaOH in 2-propanol was prepared by adding a pellet of NaOH (≈0.08 g) to 2-propanol under constant stirring at 50 °C. For a typical reaction, 8.0 mL of the zinc acetate solution was diluted to 92 mL with 2-propanol. The reaction flask was then placed in a water bath at 55 °C. Thereafter, 8.0 mL of the NaOH solution was rapidly added to the reaction flask (within 3 s) with the temperature maintained at 55 ± 2 °C. The reaction flask was isolated from the surroundings using a venting tube immersed in 2-propanol.

Preparation of Octanethiol Solution and Capping of Nanoparticles. A stock solution of the capping agent was prepared by adding 0.15 mL of octanethiol to 100 mL of 2-propanol and stirring overnight. A 1.0 mL sample of the resulting solution was injected into a 10 mL sample of the reaction solution after 10 min of growth, and to another 10 mL sample after 2 h of growth. The suspensions were immediately placed in ice water and stored under ice to quench any further reaction until absorbance spectra were obtained. The concentration of octanethiol (1.77 mM) added to the suspensions was about 1 order of magnitude larger than the concentration needed to ensure complete coverage of the nanoparticles.[6]

* Author to whom correspondence should be addressed.
[†] Department of Chemical & Biomolecular Engineering.
[‡] Department of Materials Science & Engineering.

10.1021/jp0303218 CCC: $25.00
Published on Web 08/29/2003

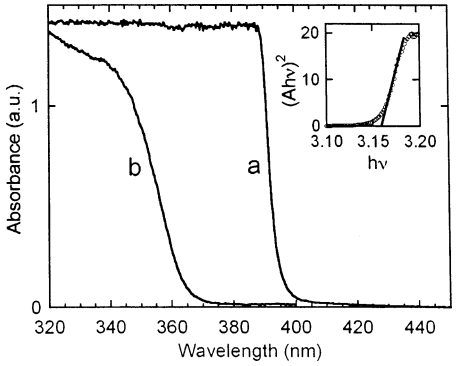

Figure 1. (a) Absorbance spectrum for (0001) ZnO single crystal and (b) absorbance spectrum for a suspension of ZnO quantum particles after 2 h of growth at 65 °C. The inset shows the spectrum for the ZnO single-crystal plotted as $(Ah\upsilon)^2$ versus $h\upsilon$.

UV Spectroscopy. Absorption spectra were recorded using a Shimadzu UV-2101PC scanning spectrophotometer. Absorption spectra for capped ZnO suspensions grown for 10 min and 2 h, respectively (described above), were recorded. Pure 2-propanol was used as the reference. Standard quartz cells (Fisher) with a 10 mm path-length were used and rinsed with 2-propanol after each run. The two samples were subsequently mixed, and the resulting solution was analyzed.

Ultracentrifugation. A 10 mL sample of a 1:1 volume mixture of the capped ZnO suspensions (average particle sizes of 1.6 and 1.9 nm, respectively) was transferred to a centrifuge tube (Beckmann, Ultra-Clear). The sample was spun at 41 000 rpm for 3 h in a Beckmann L7 Ultracentrifuge, with an SW41Ti rotor. The temperature was maintained at 1 °C to avoid any further growth or coarsening of the nanoparticles. At the end of the cycle, 3 mL of the supernatant was collected and stored in ice prior to analysis.

Evolution of Particle Size Distribution. Two ZnO suspensions with different average particle size were synthesized using the same method described above with the following differences. To obtain small particles, the reactants were mixed at 22 °C. After 4 min of growth, 35 mL of the suspension was removed, quenched in ice, and stored at 0 °C. The reaction temperature of the remaining suspension was then raised to 65 °C; after 90 min, 35 mL of the suspension was removed, quenched in ice, and stored at 0 °C. The two 35 mL samples were allowed to equilibrate at 0 °C for 1 h. The two samples were subsequently mixed in equal volumes and the reaction flask was placed in a water bath at 55 °C. Within 8 min, the reaction flask temperature rose to 55 °C and was maintained at this temperature for the remainder of the experiment. Aliquots (3 mL each) were extracted at predetermined time intervals to monitor the evolution of the particle size distribution. The reaction was allowed to proceed for 5 days at room temperature, at which point a final data point was taken.

Results and Discussion

Figure 1 shows an absorbance spectrum for a ZnO single crystal. The absorbance onset is at about 395 nm. For a direct band gap semiconductor, the absorbance in the vicinity of the onset due to the electronic transition is given by[21]

$$\alpha = \frac{C(h\upsilon - E_g^{\text{bulk}})^{1/2}}{h\upsilon} \tag{1}$$

where α is the absorption coefficient, C is a constant, $h\upsilon$ is the photon energy, and E_g^{bulk} is the band gap. From the inset of Figure 1, extrapolation of the linear region gives a band gap of 3.16 eV, close to the band gap for bulk ZnO of about 3.2 eV at room temperature.[22] Also shown in Figure 1 is a typical absorbance spectrum for a suspension of ZnO nanocrystals in 2-propanol at 65 °C. The absorbance onset is blue shifted to about 365 nm, indicating that the particles are in the quantum regime. Furthermore, the absorption edge is much broader than that for the single crystal, implying that the particle size distribution is sufficiently large that it dominates the electronic transition.

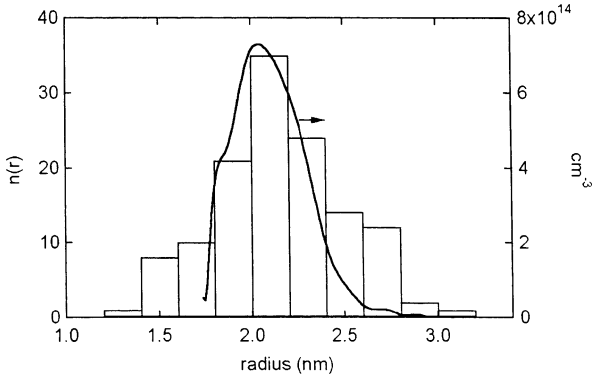

Figure 2. Particle size distribution for ZnO quantum particles after 2 h of growth at 65 °C. The histogram was obtained from analysis of high-resolution transmission electron microscope images of 125 particles. The solid line was obtained from the absorbance spectrum.

The average particle size can be determined from the absorption onset using the effective mass model:[6]

$$E^* \cong E_g^{\text{bulk}} + \frac{\hbar^2\pi^2}{2er^2}\left(\frac{1}{m_e m_o} + \frac{1}{m_h m_o}\right) - \frac{1.8e}{4\pi\epsilon\epsilon_o r} - \frac{0.124e^3}{\hbar^2(4\pi\epsilon\epsilon_o)^2}\left(\frac{1}{m_e m_o} + \frac{1}{m_h m_o}\right)^{-1} \tag{2}$$

where E^* is the band gap in eV, E_g^{bulk} is the bulk band gap, r is the particle radius, m_e is the effective mass of the electrons, m_h is the effective mass of the holes, m_o is the mass of a free electron, ϵ is the relative permittivity, ϵ_o is the permittivity of free space, $\hbar$ is Planck's constant, and e is the charge on the electron.

In the dilute concentration limit, the absorbance, A, at any wavelength in the quantum regime is related to the total volume of particles with radius greater than or equal to the size corresponding to the absorption onset. Assuming that the particles are spherical and that the absorption coefficient is independent of particle size:

$$A(r) \propto \int_r^\infty \frac{4}{3}\pi r^3 n(r)\, \mathrm{d}r \tag{3}$$

where $n(r)$ is the particle size distribution. Taking the derivative of eq 3 with respect to the particle radius, and noting that as $r \rightarrow \infty$, $n(r) = 0$, we obtain an expression relating the particle size distribution to the local slope of the absorbance spectrum:

$$n(r) \propto -\frac{{}^{\mathrm{d}A}/_{\mathrm{d}r}}{{}^{4}/_{3}\pi r^3} \tag{4}$$

Figure 2 shows a comparison of the distribution obtained from the absorbance spectrum using eqs 2 and 4, and the particle size distribution obtained from transmission electron microscopy (TEM) by measurement of 125 particles. In both cases the

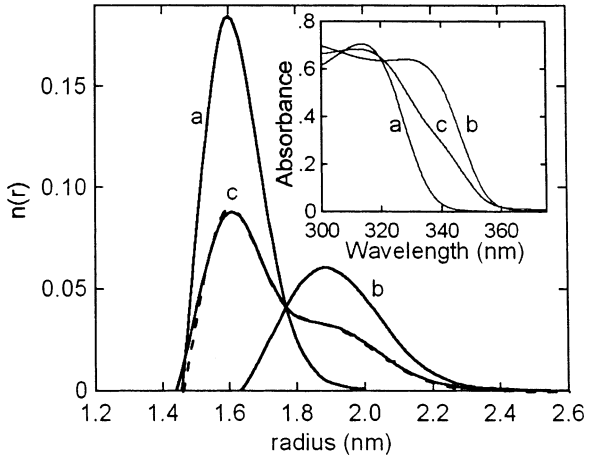

Figure 3. Particle size distribution obtained from the absorbance spectra (inset) of ZnO quantum particles with octanethiol added after (a) 10 min and (b) 2 h of growth at 55 °C. (c) Particle size distribution from a suspension obtained by mixing equal volumes of the two suspensions. The dashed line corresponds to the volume average of distributions (a) and (b).

particles were grown under the same reaction conditions and for the same time. The results obtained from our analysis show an excellent agreement with the statistical data obtained by TEM. This demonstrates that the particle size distribution can be obtained from analysis of the absorption edge. We note that the size distribution of InAs quantum dots on GaAs has been used to determine the broadening of the photoluminescence spectra.[23]

The agreement between the particle size distribution obtained from the absorbance spectrum and the distribution obtained from analysis of TEM images is poor at very small radii. This effect is due to the exciton peak in the absorbance spectra which is more pronounced for sharp particle size distributions. We note, however, that particles in this size regime comprise only a small volume fraction of the overall distribution, and we make no attempt to subtract the contribution of the exciton peak from the absorbance spectra.

The inset of Figure 3 shows the absorbance spectra for capped ZnO nanoparticles synthesized at 55 °C for 10 min and 55 °C for 2 h, respectively. Curves (a) and (b) in Figure 3 show the corresponding particle size distributions obtained from these spectra. The distributions are approximately Gaussian with peaks centered at 1.6 and 1.9 nm. Curve (c) corresponds to a mixture of equal volumes of the two suspensions. The calculated average of the individual distributions, also shown in the Figure, shows excellent agreement with the particle size distribution obtained directly from the absorption spectrum of the mixture. This result demonstrates that the precision of the absorbance measurements and accuracy in applying equation 4 are both very good.

Figure 4 shows the particle size distribution of the mixed suspension obtained from the absorbance spectra shown in Figure 3, before and after ultra-centrifugation. Larger particles experience a larger gravitational force than smaller particles, and hence they move farther down the centrifuge tube than the smaller particles. The distance that a particle moves under a centrifugal force is given by[24]

$$\ln\left(\frac{d}{d_o}\right) = \frac{4(\rho_2 - \rho_1)\omega^2 r^2 t}{18\eta} \qquad (5)$$

where d and d_o are the final and initial axial positions, respectively, ρ_1 is the density of the fluid, ρ_2 is the density of

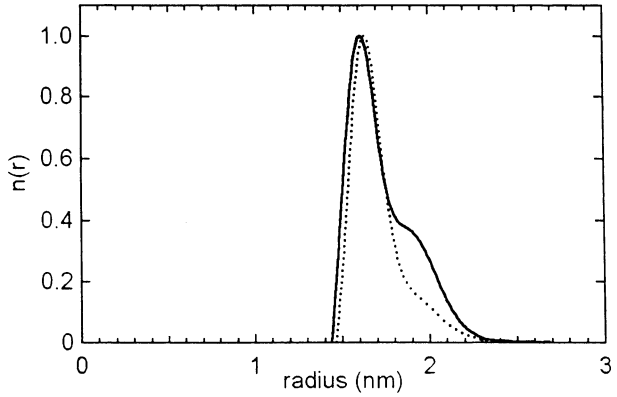

Figure 4. Particle size distribution obtained from the absorbance spectra of the mixed suspension shown in Figure 3 before (solid line) and after (dotted line) ultra-centrifugation at 41 000 rpm for 3 h at 1 °C.

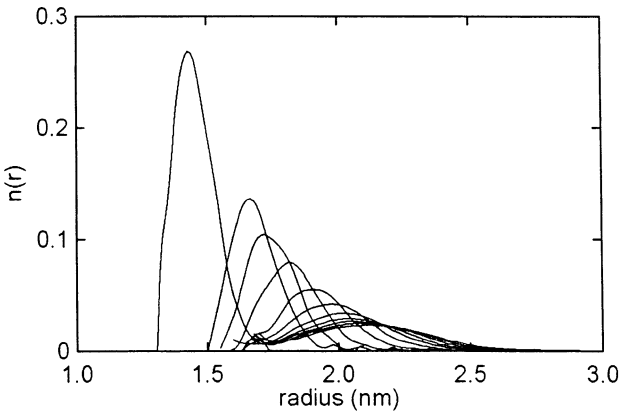

Figure 5. Evolution of an initial particle size distribution obtained from the absorbance spectra for a suspension of ZnO quantum particles coarsening at 65 °C over a period of 3 h.

the particle, ω is the angular velocity of the centrifuge, r is the radius of the particle, t is the time, and η is the viscosity of the fluid. Inserting relevant values for our system, 3 h centrifugation at 41 000 rpm would result in particles of radius 1.6 nm at the uppermost end of the centrifuge tube moving a distance of 0.92 cm and particles of radius 1.9 nm moving a distance of 1.33 cm. For this reason, 3 mL of the supernatant, corresponding to a distance of 1.95 cm from the top of the centrifuge tube, was extracted for analysis. The decrease in height of the shoulder corresponding to particles with an average size of 1.9 nm shows that a significant fraction of the larger particles are removed during centrifugation.

Figure 5 shows the evolution of the particle size distribution with time for ZnO nanocrystals grown at 65 °C using the same synthesis method described above. All particle size distributions were obtained from the corresponding absorbance spectra. Initially, a large number of particles nucleate to form a relatively narrow particle size distribution. The particles then grow until the concentration of the solute has dropped to the saturation level (within approximately 15 min) at which point the particles coarsen by Ostwald ripening.[25−28] Coarsening results in a progressive broadening of the particle size distribution as shown in numerical models of Ostwald ripening.[29,30] Due to the broadening of the particle size distribution, the height of the distribution decreases.

Figure 6 shows the evolution of the particle size distribution for a ZnO suspension grown at room temperature for 5 min (average particle size = 1.45 nm) mixed with an equal volume of a suspension prepared at 65 °C for 90 min (average particle

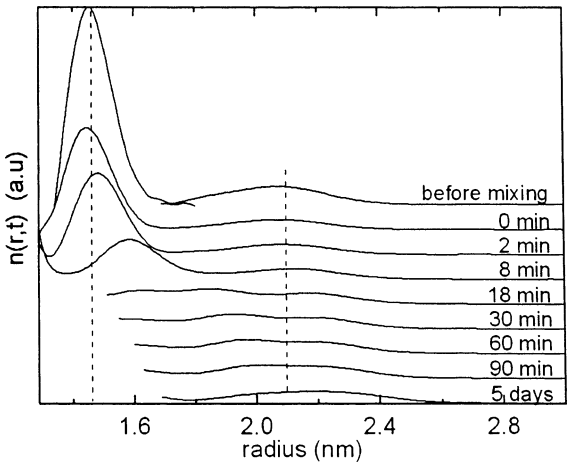

Figure 6. Evolution of the particle size distribution for a suspension containing ZnO nanoparticles grown at room temperature for 5 min mixed with nanoparticles grown at 65 °C for 90 min. Coarsening of the resulting distribution is monitored up to 5 days.

size = 2.07 nm). The volume of ZnO in each suspension is about 0.12 cm^3 per liter of 2-propanol (1 mmol L^{-1} assuming the complete reaction of zinc acetate), and hence the density of smaller particles is much larger than the density of larger particles. Thus, the sharp peak centered at about 1.45 nm is much higher than the broad peak centered at 2.07 nm.

Upon mixing ($t = 0$ min) the two suspensions, the height of the two peaks decreases by a factor of 2 due to the increased volume of solvent. After two minutes, the peak originally centered at 1.45 nm has moved to a larger radius. At the same time there is an increase in the broad peak centered around 2.07 nm. There is a dramatic decrease in height of the distribution (~60% decrease from original peak height) now centered around 1.6 nm (compared to the evolution of the distribution in Figure 5) accompanied by the loss of the smallest particles in the distribution, and the slight increase in the height of the second peak centered around 2.15 nm accompanied by the shift of the distribution to a larger average particle size. Note that the increase in radius of a larger spherical particle is less than that of a smaller particle if both particles were to take up the same mass. These features are consistent with coarsening, where large particles grow at the expense of smaller particles. After 90 min of coarsening the two distributions have almost merged, although two individual peaks are still apparent. After 5 days, the particle size distribution exhibits a single peak with no evidence of the initial bimodal distribution.

The approach described here for analysis of the absorption edge for suspensions of semiconductor nanoparticles can also be applied to other systems in the quantum regime. Many of the group II−VI and III−V semiconductors have relatively small effective masses and exhibit quantum effects up to 10 nm or more.[22,31] A notable exception is TiO_2, which has relatively large effective masses and only exhibits quantum effects at particle sizes less than 1 nm.

Conclusions

Polydispersity of zinc oxide quantum particles creates broadening of the absorbance spectrum. We confirm this relationship by inferring the particle size distribution directly from the absorbance edge and comparing it to the distribution directly measured by TEM. Further confirmation of this relationship is provided by inferring the particle size distributions of mixtures of zinc oxide nanocrystal suspensions of different sizes, and by monitoring in situ the evolution of particle size distributions. This analysis is broadly applicable to a wide range of semiconductor systems.

Acknowledgment. This work was supported by the JHU MRSEC (NSF Grant No. DMR00-80031). N.S.P. gratefully acknowledges support through a NASA graduate fellowship.

References and Notes

(1) Steigerwald, M.; Brus, L. E. *Acc. Chem. Res.* **1990**, *23*, 183.
(2) Wang, Y.; Herron, N. *J. Phys. Chem.* **1991**, *95*, 525.
(3) Kamat, P. V.; Patrick, B. *J. Phys. Chem.* **1992**, *96*, 6829.
(4) Alivisatos, A. P. *J. Phys. Chem.* **1996**, *100*, 13226.
(5) Dabbousi, B. O.; Rodiguez-Viejo, J.; Muikulec, F. V.; Heine, J. R.; Mattoussi, H.; Ober, R.; Jensen, K. F.; Bawendi, M. G. *J. Phys. Chem.* **1997**, *101*, 9463.
(6) Brus, L. E. *J. Phys. Chem*. **1986**, *90*, 2555.
(7) Brus, L. E. *J. Chem. Phys*. **1983**, *79*, 5566.
(8) Brus, L. E. *J. Chem. Phys*. **1984**, *80*, 4403.
(9) Efros, Al. L.; Rosen, M. *Annu. Rev. Mater. Res*. **2000**, *30*, 475.
(10) Andersen, K. E.; Fong, C. Y.; Pickett, W. E. *J. Non. Cryst. Solids* **2002**, *299*, 1105.
(11) Bahnemann, D. W.; Kormann, C.; Hoffmann, R. *J. Phys. Chem.* **1987**, *91*, 3789.
(12) Haase, M.; Weller, H.; Henglein, A. *J. Phys. Chem.* **1988**, *92*, 482.
(13) Spanhel, L.; Anderson, M. A. *J. Am. Chem. Soc.* **1991**, *113*, 2826.
(14) Monticone, S.; Tufeu, R.; Kanaev, A. V. *J. Phys. Chem.* **1998**, *102*, 2854.
(15) van Dijken, A.; Meulenkamp, E. A.; Vanmaekelbergh, D.; Meijerink, A. *J. Phys. Chem. B* **2000**, *104*, 1715.
(16) Wong, E. M.; Bonevich, J. E.; Searson, P. C. *J. Phys. Chem. B* **1998**, *102*, 7770.
(17) Pesika, N. S.; Hu, Z.; Stebe, K. J.; Searson, P. C. *J. Phys. Chem. B* **2002**, *106*, 6985.
(18) Hu, Z.; Oskam, G.; Penn, R. L.; Pesika, N.; Searson, P. C. *J. Phys. Chem. B* **2003**, *107*, 3124−3130.
(19) Wang, L.; Muhammed, M. *J. Mater. Chem*. **1999**, *9*, 2871.
(20) Guo, L.; Yang, S.; Yang, C.; Yu, P.; Wang, J.; Ge, W.; Wong, G. K. L. *Chem. Mater*. **2000**, *12*, 2268.
(21) Pankove, J. I. *Optical Properties in Semiconductors*; Prentice Hall: Englewood Cliffs, NJ, 1971.
(22) Berger, L. I. *Semiconductor Materials*; CRC: Boca Raton,1997.
(23) Johnson, H. T.; Nguyen, V.; Bower, A. F. *J. Appl. Phys*. **2002**, *92*, 4653.
(24) Ross, S.; Morrison, I. D. *Colloidal Systems and Interfaces*; Wiley: New York, 1988.
(25) Liftshitz, I. M.; Slyozov, V. V. *J. Phys. Chem. Solids* **1961**, *19*, 35.
(26) Wagner, C. *Z. Elecktrochem.* **1961**, *65*, 581.
(27) Ardell, A. J. *Acta Metallurgica* **1972**, *20*, 61.
(28) Marqusee, J. A.; Ross, J. *J. Chem. Phys.* **1983**, *79*, 373.
(29) Talapin, D. V.; Rogach, A. L.; Haase, M.; Weller, H. *J. Phys. Chem. B* **2001**, *105*, 12278.
(30) Smet, Y. D.; Deriemaeker, L.; Finsy, R. *Langmuir* **1997**, *13*, 6884.
(31) Shionoya, S. In *Phosphor Handbook*, Shionoya, S., Yen, W. M., Eds.; CRC: Boca Raton, 1998.